Article:
Brown, M., Pieris, D., Wright, D. et al. (2021) Non-destructive detection of machining-induced white layers through grain size and crystallographic texture-sensitive methods. Materials & Design, 200. 109472. ISSN: 0264-1275

https://doi.org/10.1016/j.matdes.2021.109472

Materials and Design 200 (2021) 109472

Contents lists available at ScienceDirect

Materials and Design

journal homepage: www.elsevier.com/locate/matdes

Non-destructive detection of machining-induced white layers through grain size and crystallographic texture-sensitive methods

M. Brown [a,g,*], D. Pieris [b], D. Wright [c], P. Crawforth [d], R. M'Saoubi [e], J. McGourlay [f], A. Mantle [f], R. Patel [b], R.J. Smith [b], H. Ghadbeigi [g]

[a] Industrial Doctoral Centre in Machining Science, Advanced Manufacturing Research Centre with Boeing, University of Sheffield, Rotherham S60 5TZ, UK
[b] Optics and Photonics Group, Faculty of Engineering, University of Nottingham, University Park, Nottingham NG7 2RD, UK
[c] Non-Destructive Evaluation, Rolls-Royce plc, PO Box 31, Derby DE24 8BJ, UK
[d] Advanced Manufacturing Research Centre with Boeing, University of Sheffield, Rotherham S60 5TZ, UK
[e] Materials & Technology development, Seco Tools AB, SE73782 Fagersta, Sweden
[f] Manufacturing Technology, Rolls-Royce plc, PO Box 31, Derby DE24 8BJ, UK
[g] The University of Sheffield, Department of Mechanical Engineering, Sir Frederick Mappin Building, Mappin Street, S1 3JD Sheffield, UK

HIGHLIGHTS

- A novel x-ray diffraction method can be used to non-destructively detect machining-induced white layers.
- The technique measures peak broadening caused by the high strain and ultra-fine grains which are intrinsic to white layers.
- White layers as small as 5 μm can be detected rapidly, compared to the time-consuming microscopy process commonly used.
- Anomalous surfaces can also be detected using laser ultrasonics, which are sensitive to crystallographic texture.

GRAPHICAL ABSTRACT

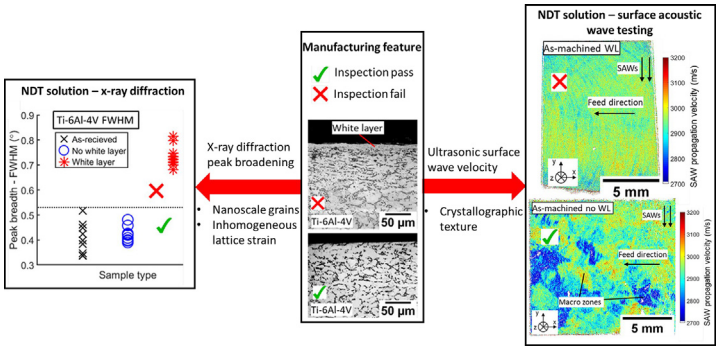

ARTICLE INFO

Article history:
Received 7 December 2020
Received in revised form 8 January 2021
Accepted 9 January 2021
Available online 11 January 2021

Keywords:
White layer
Surface integrity
X-ray diffraction
Surface acoustic waves
Non-destructive testing

ABSTRACT

Detection of machining-induced white layers is currently a destructive inspection process with a form of cross-sectional microscopy required. This paper, therefore, reports on the development of a novel non-destructive inspection method for detecting white layers using grain size-sensitive and crystallographic texture-sensitive techniques. It is shown that x-ray diffraction can be used to detect white layers as thin as 5 μm in Ti-6Al-4 V through measurement of diffraction peak breadths and diffraction peak intensities, due to the influence of the sub 100 nm grain size and high lattice strain in the white layer, as well as the strong crystallographic texture in this titanium alloy. Compared to the existing optical microscopy inspection method, which can take days due to the number of steps involved, the x-ray diffraction peak breadth method offers non-destructive white layer detection in a matter of minutes at a resolution of 5 μm or less that competes directly with the optical method. Spatially resolved acoustic spectroscopy, a laser-generated ultrasonic surface acoustic wave detection method, can also be used to identify anomalous surfaces, containing a white layer or swept grain material, due to its sensitivity to the crystallographic texture changes that arise in severely plastically deformed Ti-6Al-4V as in Titanium with 6 % Aluminium and 4% Vanadium.

* Corresponding author at: Advanced Manufacturing Research Centre with Boeing, University of Sheffield, Rotherham S60 5TZ, UK.
E-mail address: m.o.brown@sheffield.ac.uk (M. Brown).

https://doi.org/10.1016/j.matdes.2021.109472

1. Introduction

Machining is used to produce the desired final shape and surface finish during the manufacturing of most aeroengine components, including blades and shafts. Aeroengine alloys, such as titanium, which is used for the lower temperature components such as the fan blades, are considered difficult-to-machine materials due to their high strength and low thermal conductivity which results in the localisation of heat generation and shear deformation in the near-surface region during machining, as reported by Ezugwu et al. [1]. This localisation has a direct impact on the resultant surface integrity of the component, in particular, white layers, an anomalous surface integrity feature, can be generated in the near-surface region when machining at high cutting speeds or increased levels of tool wear as shown by Che-Haron and Jawaid [2].

White layers are typically classified as a region in the near-surface of a material in which the microstructure cannot be resolved with optical microscopy, even at high magnifications. These layers typically form in machined surfaces by either a thermally-dominated phase transformation mechanism, or a severe plastic deformation-dominated mechanism [3]. When machining titanium alloys with worn tools, white layers have been measured by Brown et al. [4] to be composed of ultra-fine grains, possess higher hardness than the bulk material and have a strong basal hexagonal close-packed (HCP) texture. White layers themselves cannot be associated with a particular residual stress state, however, the machining conditions which lead to their formation, high cutting speeds or high tool wear, often result in considerable tensile [5] or compressive residual stresses [4] respectively. It has been shown by Herbert et al. [6] that the presence of a white layer in a nickel superalloy can cause a 10 times reduction in the low cycle fatigue life of a component even after shot-peening. Poulachon et al. [7] have shown that white layers can be brittle and as such, their presence would lead to an inspection failure in an aeroengine component, regardless of the residual stress state or alloy type. A swept grain region, in which the near-surface material is distorted in the direction of machining, is typically found beneath a white layer, as highlighted by Brown et al. [4], and is also considered detrimental to the surface integrity, due to the associated decrease in the fatigue life of a machined component that has been measured by Hardy et al. [8].

Current methods for white layer detection in industry are destructive as typically the component to be tested is sectioned, mounted, polished and etched before being inspected with optical microscopy [9]. This process, whilst effective for capturing anomalous surfaces, is inherently costly, due to the parts that are sacrificed and the time-consuming nature of the steps involved in preparing a sample for inspection. It also leads to parameter-frozen processes with changes only implemented after full part validations. As such, there is a desire within industry to be able to detect white layers non-destructively to speed up and reduce the cost of inspection. NDT techniques also offer the potential for in-process monitoring and therefore align with the aims of smart factories. In this study, x-ray diffraction (XRD) and spatially resolved acoustic spectroscopy (SRAS) methods are employed to non-destructively inspect machined Ti-6Al-4 V samples with and without white layers, utilising the sensitivity of the techniques to the intrinsic properties of white layers, a small grain size and a strong crystallographic texture.

Machining-induced white layers have previously been detected non-destructively in steels using the ferromagnetic Barkhausen noise inspection method by Stupakov et al. [10] and Brown et al. [11], however, this technique is not transferrable to paramagnetic aeroengine materials such as titanium alloys and nickel superalloys. Stupakov et al. [10] could rank samples according to the level of white layer thickness by measuring the height of a second peak in the Barkhausen noise at higher magnetic field strengths. This was attributed to a harder white layer than the softer dark layer beneath, a favourable orientation of the martensitic matrix in the white layer and an increasing volume of retained austenite with a thicker white layer. However, these are properties associated with white layer formation through thermally dominant mechanisms [12] so the technique may not be transferable to severely plastically deformed white layers. Brown et al. [11] were able to separate all surfaces with a white layer thicker than 2 μm from those with thinner or no white layers by measuring the frequency at which peak Barkhausen noise occurred. However, the technique was found to be primarily sensitive to the residual stress state rather than an intrinsic property of the white layers.

At the time of writing, there has been only a limited number of studies into the specific detection of white layers in non-magnetic alloys. Guo and Ammula [13] attempted to monitor white layer formation during the turning of hard steels using acoustic emission testing. It was proposed that the root mean square and frequency of the acoustic signal could be used as key indicators for the onset of white layer generation in the machined surface, however, it should be noted that surface roughness, tool edge sharpness and white layer formation are all reported to affect the signal. As such, it is difficult to extract the proportion of the signal which is specifically due to white layer formation.

Daghini et al. [14] have claimed that the increase in the amount of optical scattering on a surface machined with worn insets can be attributed to the presence of a white layer rather than an increase in surface roughness which was similar across all the samples tested. This indicates that optical scattering could be appropriate as a test for white layer, however, only 4 samples and one type of alloy were investigated so further study is necessary to instil greater confidence in the presented results, particularly when no clear link has been presented between the technique and the key properties of a white layer.

In one study, Patton et al. [15] investigated the use of non-destructive testing (NDT) methods for the detection of broader machining damage in Ti-6Al-4 V. It was identified that XRD measurements could be used to detect metallurgical machining damage, a subdivision of surface integrity, which encompasses white layers, among other anomalous features. This detection was facilitated by different diffraction peak intensity attributed to machining damage. Based on the crystallographic texture of Ti-6Al-4 V white layers identified by Brown et al. [4] it can be predicted that the change in peak height could have been due to the presence of a white layer. In a preliminary study, Brown et al. [4] investigated the potential for applying XRD as a method for the detection of machining-induced white layers in Ti-6Al-4 V. It was found that for the limited number of samples inspected, those with a white layer resulted in a relative increase of the measured intensity of the basal $\alpha\{0002\}$ peak to the pyramidal $\alpha\left\{10\bar{1}1\right\}$ peak, compared to samples with no white layer. As such, there is merit for further investigation into specific white layer detection using XRD intensity measurements in this alloy.

In addition to the diffracted x-ray peak intensity, the diffraction peak breadth can also be measured. It is well documented that XRD peaks broaden when the diffracting domain size is small (<200 nm) and there is inhomogeneous lattice strain [16] and as such, the broadening of XRD peaks can be used as a measure of diffraction domain size. The diffraction domain size is often equivalent to the grain size in polycrystalline materials, however, for severely plastically deformed (SPD) material produced by processes such as equal channel angular compression and high-pressure torsion, the domain size can be six times smaller than the grain size measured by TEM as shown by Zhilyaev et al. [17]. Ungár et al. [18] attributed this discrepancy to the presence of dislocation cells within grains, with low angle boundaries between cells. This misorientation cannot be observed using TEM contrast imaging, however, XRD is sensitive to it.

The broadening of XRD peaks has been used by Baumann et al. [19] to measure the grain size in a steel alloy when a white layer was formed

on the surface due to friction and wear arising from the rail-wheel contact. It is worth noting that the XRD method was not used for non-destructive assessment, instead, it was merely adopted as a way of characterising the white layer and as such required destructive sectioning. The ultrafine grain size of the white layer across all aeroengine alloys can be used to infer that the measurement of the XRD peak breadth may be a useful method for the detection of anomalous surfaces.

In addition to XRD, results presented in the literature indicate that ultrasonic, specifically surface acoustic wave (SAW) detection methods, may be applicable to white layer detection due to the sensitivity of the propagation velocities of the generated SAWs to the crystallographic texture of the material under inspection. Patton et al. [15] used the measurement of the backscatter angle of SAWs to detect metallurgically damaged surfaces, with the distinction to undamaged surfaces facilitated by a change in backscatter angle and therefore SAW propagation velocity which was attributed to a change in the elastic modulus of the surface region, but not explored further or attributed to a specific surface integrity feature. The basal texture measured in Ti-6Al-4 V white layer machined with worn inserts [4] is the most likely cause for the reported change in SAW propagation velocity, due to the anisotropy of the α-Ti HCP crystal which can result in changes in elastic modulus of up to 45% between different crystal orientations as measured by Larson and Zarkades [20]. Farnell [21] has shown that the propagation velocity of a SAW on a HCP basal plane is uniform in all directions and faster than on other planes.

Laser generated SAWs have been used by Smith et al. [22] to detect surfaces and sub-surface defects within manufacturing components. Due to their inherent non-destructive and non-contact nature, laser generated SAWs can be used in environments with limited access [23], elevated temperatures [24] and on components with rough surfaces [25]. These systems can be arranged to work with various wave modalities (shear, longitudinal, surface) where surface waves are typically used to measure the properties at the surface of a component. The technique used in this paper, SRAS [26], is a laser-ultrasonic technique which robustly measures the SAW velocity and is capable of microstructure and crystallographic texture measurements in a variety of materials such as nickel and titanium, and with a range of surface conditions from mirror finish to the very rough surfaces found on additively manufactured components, as shown by Patel et al. [25].

It is apparent from the review of the existing literature that a non-destructive method which could detect white layers in different alloys would be beneficial in industry to reduce inspection time and the cost associated with sacrificing components. Presently, only white layers in ferromagnetic materials can be detected non-destructively, as such, a method which is sensitive to this surface integrity feature in both ferromagnetic and non-ferromagnetic materials would be beneficial, particularly as it has been shown that white layers can readily form in all difficult-to-machine metals. Whilst previous work in non-ferromagnetic alloys, such as the extensive study by Patton et al. [15], have focused on detection of general machining damage, the intrinsic properties of white layers that differentiate it from other surface integrity features, such as its highly refined grain size, necessitate an experimental approach focused on sensitivity these properties to maximise the white layer inspection capability.

In this study, we present development of XRD peak breadth and XRD intensity ratio methods for novel non-destructive detection of white layers in machined aeroengine alloys, in addition to a SRAS method for detecting a machined Ti-6Al-4 V component with poor surface integrity. Results from the NDT measurements are discussed in the context of the texture and microstructure properties of the white layers. This paper aims to assess the feasibility of using XRD and SAW techniques as NDT methods for the detection of machining-induced white layers in aero-engine components, thereby reducing the need for destructive microscopy assessment and enabling the possibility of in-process inspection and validation of production components.

2. Experimental methods

To investigate the potential for the non-destructive inspection of white layers, machined surfaces containing white layers had to be generated. The methods to generate these surfaces and the conditions for the XRD and SRAS inspection are outlined in this section.

2.1. Machining trials

Single-point square shoulder-milling machining trials were used to generate Ti-6Al-4 V surfaces containing white layers, with thicknesses between 5 and 20 μm. Machining was carried out using a Mori-Seiki Nv5000α1 vertical machining centre with a Seco Tools shoulder milling cutter (R217.69–2020.0-12-2AN) and coated tungsten carbide inserts (XOEX120408R-M07 MS2050), some of which had been ground to introduce artificial levels of flank wear beyond 0.5 mm. Cutting speeds of 20–200 m/min, a feed rate of 0.06 mm/tooth an axial depth of cut of 16 mm and radial depths of cut between 0.5 and 2 mm were imposed in the trials. A schematic of the milling operation is shown in Fig. 1. Following machining, the workpieces were sectioned to produce samples for XRD and SRAS inspection (machined surface samples) as well as materials characterisation (cutting and feed direction samples) from adjacent regions. For materials characterisation, the cross-section of each sample was polished and etched to reveal the microstructure with the surface integrity quantified using an optical microscope. Full quantitative characterisation of the machined workpieces has been described previously [4], this included scanning electron microscopy, XRD phase analysis and pole figure measurements, residual stress profiling and nanoindentation.

Additional samples for validation tests in different materials were created by square shoulder milling IN-718, a nickel superalloy, and turning super chrome molybdenum vanadium (SCMV), an aerogengine shaft steel. The Inconel-718 surfaces were machined using the same set-up as for the Ti-6Al-4 V samples but with cutting speeds in the range 20–80 m/min. SCMV turning was undertaken on a Cincinnati Hawk 300 lathe using a PDJNL2020K15JETL tool holder in combination with DNMG 150608 coated carbide inserts, both provided by Seco tools AB. Quantitative characterisation of these SCMV workpieces has been described previously in a previous investigation into non-destructive white layer detection using Barkhausen noise inspection [11].

2.2. XRD-ΔPB method

XRD-ΔPB (peak breadth) measurements on machined surface samples (as defined in Fig. 1) were carried out using a PANalytical Xpert^3 powder diffractometer equipped with a copper Kα x-ray tube. An initial investigation, to identify the most suitable diffraction peaks for

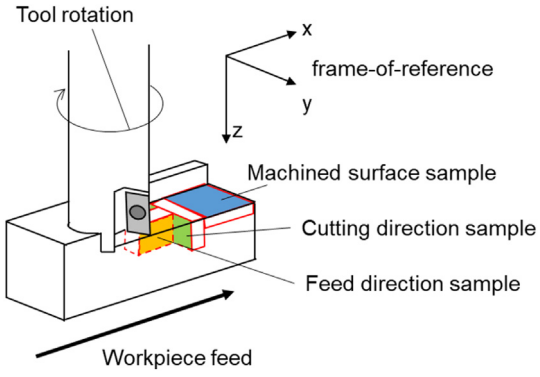

Fig. 1. A simplified schematic of the milling operation highlighting the samples used for microstructure characterisation (cutting and feed direction samples) and samples used for NDT (machined surface samples).

detecting white layers through peak breadth measurements, was undertaken for diffraction angles between 30 and 130° using a step size of 0.0131°. Post-processing was carried out on the resulting XRD pattern using PDF-4+ software [27]. Background intensity and high-frequency noise were removed but the low-frequency shape of the diffraction peaks was preserved. It should be noted that the Xpert^3 required parts to be sectioned to fit within the confines of the diffractometer, however, the method is transferrable to other equipment which facilitates truly non-destructive inspection. As such, results from validation tests using other diffractometers are reported in this paper.

Peak broadening in XRD arises due to a combination of three main factors, crystallite size, inhomogeneous lattice strain and instrument broadening, as outlined by Cullity [16]. To remove the effect of instrument broadening when selecting the most appropriate diffraction peak, the peak breadths were corrected using measurements from an annealed Ti-6Al-4 V sample with large grains. The full width at half-maximum (FWHM), was used as the peak breadth measure, rather than integral breadth. This is because Scardi et al. [28] have shown that FWHM is more suited for situations where tail peaks are overlapping, as was encountered in these measurements for some peaks due to the high level of broadening in a number of samples.

Following the identification of suitable diffraction peaks, further measurements were carried out on a larger number of machined surfaces, with only the $\alpha\left\{10\bar{1}1\right\}$ diffraction peak targeted. Diffracted x-ray intensity was captured for diffraction angles between 37 and 42°. The XRD peak breadth measurement itself is highly repeatable, the same sample inspected twice without remounting was found to have a peak breadth variation smaller than 1% between measurements. However, XRD is sensitive to small variations in the sample mounting, including the sample height and tilt relative to the x-ray beam. To check for erroneous mounting, each sample was measured twice, with the sample remounted before the second measurement. A discrepancy greater than 0.05° between the peak breadths was used as an indicator of a sample at the wrong height or tilt and the measurements were repeated. The peak breadth measurement was then taken as the average of two measurements.

A modified Williamson-Hall (W-H) method, as described by Shafi and Bose [29], which considers the effect of strain anisotropy, was used in an attempt to decouple the effects of crystallite size and inhomogeneous lattice strain on peak broadening. This strain anisotropy W-H method accounts for the variation in elastic modulus across different crystallographic planes.

2.3. XRD-ΔIR method

To investigate the potential for detecting white layers in Ti-6Al-4 V through the effect of their strong {0002} texture on an XRD pattern, intensity measurements of the {0002} peak were compared against the adjacent $\left\{10\bar{1}1\right\}$ peak for machined surface samples. The intensity ratio (IR) of these two peaks, as defined in Eq. 1, was used to facilitate comparison between samples with and without white layers, with reference to any measured differences in the crystallographic texture reported during previous destructive characterisation [4]. The intensity ratio measurement was repeated with the sample remounted and a difference exceeding 10% between measurements was used to indicate sample-mounting errors.

$$IR = \frac{I_{\{0002\}}}{I_{\left\{10\bar{1}1\right\}}} \tag{1}$$

To determine the resolution capability of both XRD methods for detecting white layers, additional machined surfaces were electropolished to remove material from the white layer, thereby creating samples with thinner white layers, without introducing mechanical deformation. These electropolished surfaces were inspected with XRD before the white layer thickness of each sample was quantified through cross-sectional optical microscopy.

To validate both XRD methods, additional machined surface samples with and without white layers SCMV and Inconel-718 were tested. The diffraction peaks used for peak breadth measurements were the $\gamma/\gamma'/\gamma''\{200\}$ peak in Inconel-718 and the $\alpha/\alpha'\{211\}$ peak in SCMV.

X-rays penetrate only a limited depth into a material due to energy loss via collisions with atoms in the material [16]. The approximate depth of inspection in each material, taken as the depth at which 90% of x-rays are attenuated, was calculated from the composition of each alloy, the corresponding mass attenuation coefficients obtained from Hubbell [30], the diffraction angle and the material density and is shown in Table 1. The illumination area of the x-ray beam was approximately 4 mm × 8 mm across all samples which is considerably larger than the average grain size in the white layer (sub 100 nm) and bulk (sub 30 μm).

2.4. SRAS

The SRAS technique uses a broadband pulsed infrared (1064 nm) laser to thermoelastically generate a SAW on the surface of a sample. The frequency (f) of the generated SAW is controlled by the spacing of the grating pattern (fixed wavelength (λ)) imaged onto the material surface [26]. The acoustic velocity of the material under the generation patch means that only a specific frequency wave will be generated by the instrument. The surface perturbation caused by the propagation of the SAW across the material surface is measured using a continuous wave green (532 nm) detection laser in conjunction with a knife-edge detector. The velocity of the detected SAW (v_{SAW}) is calculated using Eq. 2, where f and λ are the frequency and wavelength of the generated SAW, and can be used to measure changes in material properties, such as measuring sub-surface defects [22], or microstructure [31]. In the latter case, the material's elastic modulus changes with the crystallographic orientation which changes the measured SAW velocity.

$$v_{SAW} = f\lambda \tag{2}$$

The type of SAW generated is dependent on the material interface and thickness, for an infinite half-space made of a single material, a Rayleigh wave is generated [32]. The properties of the white layer are different from the bulk material and so the white layer can be viewed as a thin layer on a substrate akin to a coated sample. Detection of SAW velocity changes due to sample coating has been reported by Patel et al. [33] and a similar shift in velocity is expected for white layers depending on their thickness. The individual particle motion shown in Fig. 2 demonstrates how the SAW wave propagates into the material, the particle motion decays exponentially as the depth increases meaning that the largest influence on the measured velocity is from the material approximately one acoustic wavelength from the surface.

To prepare samples for SRAS, 10–15 mm square blocks were sectioned from the workpieces, adjacent to samples used for microscopy analysis as highlighted in Fig. 1, and then mounted in Bakelite, before being polished to a mirror finish. Material removal was quantified using a digital micrometre accurate to 2 μm, to prevent the complete removal of the white layer during polishing. It was not possible to avoid mechanical polishing of the white layers, due to the need for an optically

Table 1
Approximate inspection depths for each alloy examined during the XRD measurements.

Material	2θ (°)	Inspection depth (μm)
Ti-6Al-4 V	40.5	4.6
Inconel-718	50.5	4.1
SCMV	82	3.2

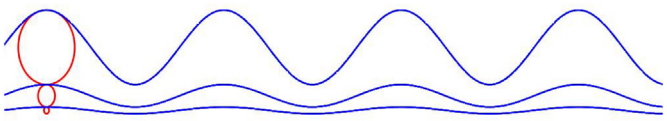

Fig. 2. Figure illustrating the decrease in amplitude of the SAW wave (blue line) with depth and the circular particle motion (red circles). (For interpretation of the references to colour in this figure legend, the reader is referred to the web version of this article.)

smooth surface with the SRAS instrumentation used in this study, however the technique is applicable to rough surfaces with a rough surface detector [25].

In this study, the SRAS measurements were obtained using a generation patch with a diameter of 200 μm and a wavelength of 24 μm. The detection laser spot had a diameter of ~8 μm and was positioned at the edge of the generation patch. The generation and detection lasers were raster-scanned across the surface of the sample with a step size of 20 μm and 40 μm in x/y direction respectively. The frequency of the acquired waveforms was extracted with a Fast Fourier Transform and then by using $v = f\lambda$ the velocity was calculated and mapped into an image representing the full surface under inspection.

2.5. Depth-profiling

To facilitate a direct comparison between the SRAS and the XRD-ΔPB methods in different material regions, from the white layer through to the bulk material, a machined sample was ground and polished using P2500 grit paper and a Struers MD Chem polishing pad with colloidal silica suspension. At every depth interval, the surface was scanned with SRAS and inspected with the XRD-ΔPB method. This process was repeated at depth intervals, quantified using a digital micrometre, through the white layer region and the distorted material beneath until only the bulk material remained. The XRD-ΔIR method was not investigated, due to the effect of mechanical polishing on the resultant texture, which could alter the texture of the near-surface region. It should be noted that the strain introduced by mechanical polishing may also influence peak breadth measurements, however, the polishing process was the same for all layers so any peak breadth change with depth must be attributed to another factor.

3. Results

The two NDT methods were initially analysed separately before comparing the techniques on a sample that was subjected to successive layer removal from the white layer region through to the bulk material.

3.1. X-ray diffraction

3.1.1. XRD-ΔPB

The results from the initial XRD-ΔPB inspection of six Ti-6Al-4 V machined surfaces, to enable diffraction peak selection, are presented in Fig. 3. In these samples, a full diffraction pattern was captured and the peak breadth for each peak was calculated. In all samples with a white layer, the layer thickness was greater than the depth of penetration of x-rays. It can be seen that samples with a white layer exhibit a larger peak breadth than samples with no white layer for all peaks except α{0002} and α{0004}, which are 1st and 2nd order diffraction peaks of the same crystallographic plane. Peaks corresponding to the $\alpha\{10\bar{1}1\}$, $\alpha\{11\bar{2}0\}$ and $\alpha(20\bar{2}3)$ planes show the greatest change in peak broadening between samples with and without white layers, as highlighted in Table 2. The uncertainty was calculated based on the standard deviation of the measurements on white layer and non-white layer surfaces.

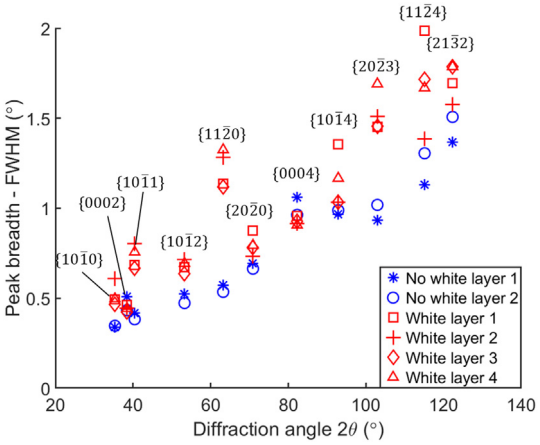

Fig. 3. FWHM peak broadening for peaks corresponding to different crystallographic planes.

Table 2
The percentage increase in measured peak breadth when a white layer is present for peaks of interest.

Peak	2θ (°)	*FWHM* PB/PB difference (%)
$(10\bar{1}1)$	40.5	82 (±9)
$\{11\bar{2}0\}$	63.2	120 (±18)
$\{20\bar{2}3\}$	103.0	56 (±17)

The optimum peak for white layer detection provides a large percentage change in measured values between samples with and without white layer, whilst also facilitating a fast measurement through a strong diffracted x-ray signal. The relative intensities of each peak are highlighted in a diffraction pattern of the as-received material, as shown in Fig. 4. It can be identified that the $\alpha\{11\bar{2}0\}$ peak has a lower peak intensity than the $\alpha\{10\bar{1}1\}$ peak and, as such, would require longer scan times to produce the same peak intensity, increasing the overall inspection time if used as an NDT method for white layer inspection. For this reason, the $\alpha\{10\bar{1}1\}$ peak was selected to take forward for further investigation as it provides a large distinction between surfaces with and without a white layer but also offers a

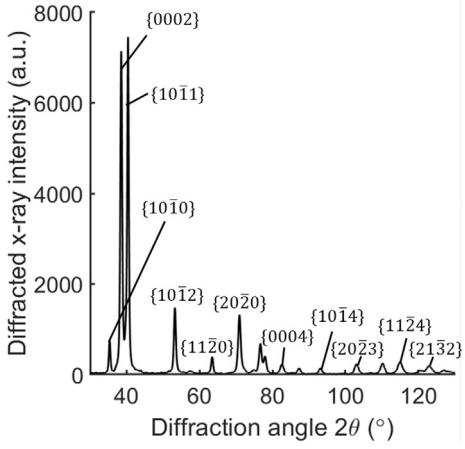

Fig. 4. A diffraction pattern for a solid titanium sample with the peaks used for peak broadening analysis highlighted.

shorter scan time than for the $\alpha\{11\bar{2}0\}$ peak. However, the peak breadth method could be applied to the majority of XRD peaks.

Quantitative FWHM peak breadth measurements in the full set of machined surfaces with and without a white layer, using the $\alpha\{10\bar{1}1\}$ diffraction peak, are shown in Fig. 5(a), in addition to measurements from examples of as-received material with different crystallographic orientations. Example micrographs of surfaces with and without a white layer are provided. The XRD peak broadening method facilitates the detection of surfaces containing a white layer in all the Ti-6Al-4 V test pieces examined. It is apparent that a threshold value between 0.53° and 0.66° in this specific combination of test-piece material and diffractometer set-up, would allow anomalous surfaces to be identified. No relationship appears to exist between the measured peak breadth and the underlying white layer thickness as shown in Fig. 5 (b). However, the white layer thickness is greater than the depth of penetration of x-rays in these samples.

3.1.2. XRD-ΔIR

The results from XRD-ΔIR measurements of the same set of Ti-6Al-4 V samples are presented in Fig. 6(a). It can be seen that samples containing a white layer are distinguishable from samples with good surface integrity and examples of as-received material with a threshold IR value of 1.9 indicative of a surface containing a white layer. The intensity ratio, even in textured as-received material, such as uni-directionally rolled plate, was not sufficient to trigger an anomalous white layer measurement. Similar to the peak breadth measurements, the intensity ratio was not measured to be proportional to white layer thickness, as shown in Fig. 6(b).

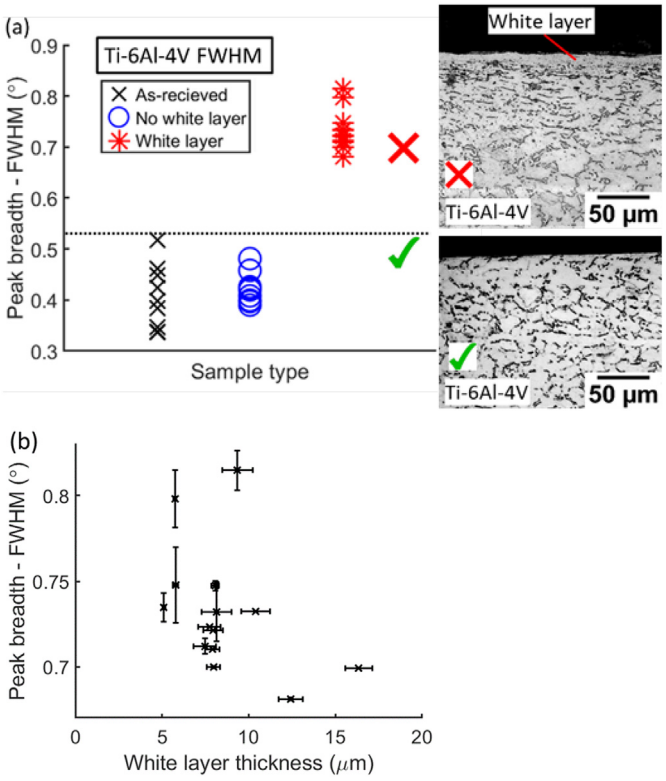

Fig. 5. Plots of (a) the peak breadth plotted against the sample type and (b) the peak breadth plotted against the white layer thickness. Error bars represent the standard deviation in the peak breadth and thickness measurements.

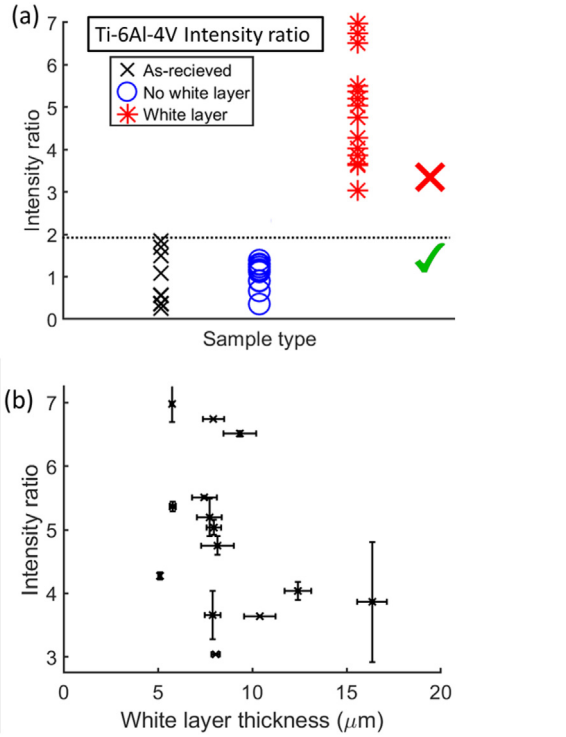

Fig. 6. Plots of (a) The intensity ratio measured for different machined surface samples and (b) the dependence of intensity ratio on white layer thickness. Error bars represent the standard deviation in the intensity ratio and thickness measurements.

3.1.3. The effect of white layer thickness on detection capability

By reducing the white layer thickness, through electropolishing, such that it was smaller than the x-ray interaction depth, the peak breadth was measured to be related to the white layer thickness. A lower peak breadth can be associated with thinner white layers, as shown in Fig. 7. This is to be expected due to the increased x-ray diffraction contribution from the non-white layer material, which has a lower peak breadth, as shown previously in Fig. 5(a). It should be noted that these results suggest that accurately predicting the white layer thickness from peak breadth measurements is not possible across all machined surfaces. This is evident from Fig. 7 where it can be seen that a single peak breadth value can be associated with different white layer

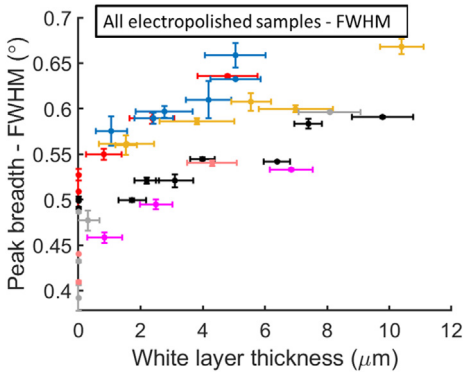

Fig. 7. Peak breadth plotted against white layer thickness for electropolished surfaces. Each colour and marker shape corresponds to electropolished samples from a particular machined surface. Error bars represent the standard deviation in the peak breadth and thickness measurements.

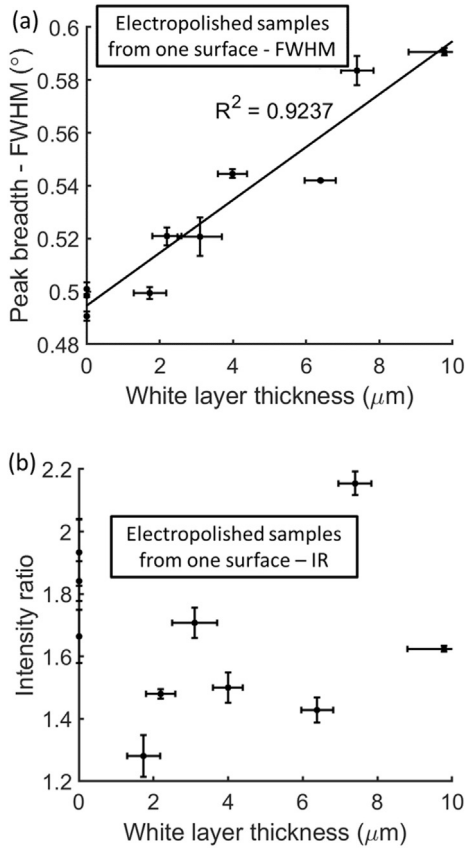

Fig. 8. Plots of (a) Peak breadth and (b) intensity ratio against white layer thickness for electropolished samples from a single machined surface. Error bars represent the standard deviation in the peak breadth, intensity ratio and thickness measurements.

thicknesses, depending on the sample under inspection. The peak broadening varies for different machined surfaces due to differences in the grain size in the white layer and the lattice strain imparted at different cutting conditions, even when a white layer is not present.

Focusing on samples from just one machined surface, as plotted in Fig. 8(a), the decrease in peak breadth for thin white layers is more apparent with a narrow distribution of points about a linear fit ($R^2 = 0.92$). By contrast, intensity ratio appears to be independent of the white layer thickness, as indicated by the results shown in Fig. 8(b), where there is considerable variation within a single machined surface ($R^2 = 0.01$).

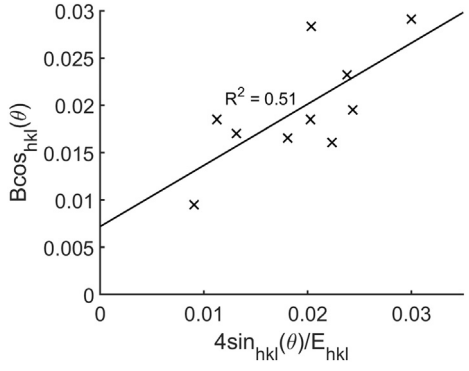

Fig. 9. A modified W-H plot, considering strain anisotropy, for a sample with a white layer.

3.1.4. The effect of crystallite size and inhomogeneous lattice strain on XRD peak breadth

Results from the modified W-H investigation into the relative effects of crystallite size and inhomogeneous lattice strain broadening on the overall peak breadth, in surfaces containing a white layer, are shown in Fig. 9. It can be seen that the data does not fit the linear relationship well, due to the considerable scatter of the points, as indicated by the R^2 value for a linear fit. Additional surfaces, both with and without white layers, were examined using the same methods with varying quality of fits, with R^2 values above and below the examples presented here. The poor fit and large variability between samples meant that predictions of the relative effects of crystallite size and inhomogeneous lattice strain could not be made with confidence. However, it can be seen that qualitatively, the fit has a positive gradient and this is indicative that inhomogeneous lattice is contributing to peak broadening, alongside the ultrafine grains known to be present in the white layer.

3.1.5. XRD technique validation

To validate both XRD methods for other aeroengine alloys, further XRD tests were undertaken on Inconel-718 and SCMV machined surfaces, as shown in Table 3. It can be seen that it is possible to detect a surface with a white layer in these other materials using XRD-ΔPB measurements. In both alloys, a surface with a white layer results in the considerable broadening of the XRD peak compared to a sample that would pass surface integrity inspection. The results from α{111}/{200} intensity ratio measurements in Inconel-718 surfaces are shown in Table 3, it can be seen that this method is also effective at detecting white layers in nickel superalloys. However, no combination of peaks proved successful for intensity ratio inspection in SCMV. Example micrographs of white layer and non-white layer surfaces in both alloys are shown in Fig. 10.

To demonstrate a truly non-destructive test for white layers using XRD by removing the need for sectioning to fit in the Xpert[3] diffractometer, additional measurements were carried out using a PANalytical Empyrean diffractometer and a proto iXRD diffractometer, as shown in Fig. 11 (a) and (b). It is important to note that the iXRD is limited to high-angle diffraction peaks, consequently, the 140° $\alpha\{21\bar{3}3\}$ peak was used for peak breadth measurements. A molybdenum x-rays source was used in the Empyrean tests to demonstrate that white layer detection is not restricted to copper x-ray radiation. Different radiation sources can be used to alter the x-ray penetration depth. The peak breadths for measurements on a single sample of each type of surface using the Empyrean and the iXRD are shown in Table 4. The results from the analysis of each type of sample indicate that the peak breadth method for white layer detection is transferrable between different equipment and can, therefore, be truly non-destructive.

3.2. SRAS

3.2.1. Velocity maps

The SAW velocity distribution across a test piece is dependent on the underlying surface integrity, as shown in Fig. 12(a), (b) and (c). For both as-received material and machined surface samples with good surface integrity, Fig. 12(a) and (b), the velocity maps reveal regions of similar velocities across the surface. These regions arise due to the macroscopic texture of the workpiece material, whereby similarly orientated regions of material arising from the prior processing route are mapped as the predominant velocity at the inspected point. By contrast, for a surface that has been machined with worn inserts, the macro-texture of the workpiece is destroyed, resulting in a velocity map that is more amorphous, as shown in Fig. 12(c).

3.2.2. Microscopy

Optical micrographs from cutting direction samples corresponding to different regions across a machined surface sample are highlighted

Table 3
Results from peak breadth and intensity ratio inspection in Inconel-718 and SCMV validation samples.

Surface	White layer present ✗	White layer not present ✓
FWHM – Inconel-718 (°)	1.11 (±0.01)	0.732 (±0.05)
FWHM – SCMV (°)	1.19 (±0.06)	0.86 (±0.09)
IR – Inconel-718	15.25 (±2.40)	2.24 (±0.83)
IR – SCMV	Overlap between samples	

in Fig. 13 alongside a SRAS velocity map from the same surface. It can be seen that the higher velocity regions, at the top and bottom of the velocity map, correspond to regions with increased white layer thicknesses, relative to the central region. As the thickness of the white layer (5–7 μm) is thinner than the SAW wavelength (24 μm), the velocity map is also significantly influenced by the swept grain region beneath the white layers.

3.3. A comparison between SRAS and XRD methods for white layer detection

The results from SRAS measurements at successive depths, on a machined surface sample that originally contained a 10 μm thick white layer, are shown in Fig. 14. It can be seen that in the immediate subsurface, at a depth of approximately 6 μm, the measured velocity map appears amorphous, with no macrozones visible, similar to the velocity map shown in Fig. 12(c). In the data gathered between 6 μm and 23 μm below the machined surface, the cutting tool arcs are visible and regions of lower velocity are more apparent. These marks cannot be the physical feed marks left behind following machining, as these were no larger than 1 μm yet 23 μm of material has been removed to create the depth profile sample. These arcs must, therefore, be present within the material microstructure and this is explored further in the discussion section. Moving to 44 μm beneath the machined surface, macrozones can be resolved but there are still arcs visible, indicating a machining-affected region. Beyond this depth, in the velocity map at 99 μm beneath the surface, the macrozones observed in the as-received material become fully visible, and the cutting arcs cannot be resolved.

A comparison between the XRD peak breadth and the average SRAS velocity across all four scan directions during the depth profiling experiment is shown in Fig. 15. It can be seen that both methods are sensitive to a change in the measured property with increasing depth beneath the machined surface. The peak breadth more than doubles between the bulk material and a surface with a white layer and this is a much greater change than the corresponding 6% increase in average SRAS velocity, relative to the range of expected values for the propagation of a SAW in HCP titanium. Additionally, the standard error for the SRAS measurements (up to 22 m/s), highlighted by the error bars in Fig. 15, is greater than for the XRD measurements, which had an error smaller than 0.02° due to the high repeatability of XRD highlighted previously. However, the SRAS measurement also captures the spatial distribution of the velocity as illustrated previously in Fig. 14 and it is this distribution that is more beneficial for assessing the surface integrity using SRAS compared to the average velocity.

4. Discussion

The results presented in this study indicate that x-ray diffraction can be used to detect machining-induced white layers in Ti-6Al-4 V via the XRD-ΔPB or XRD-ΔIR method. The measurements on validation samples highlight the transferability of the XRD-ΔPB technique to other materials, equipment and x-ray sources, with only an adjustment to the threshold values required. This broad material applicability is

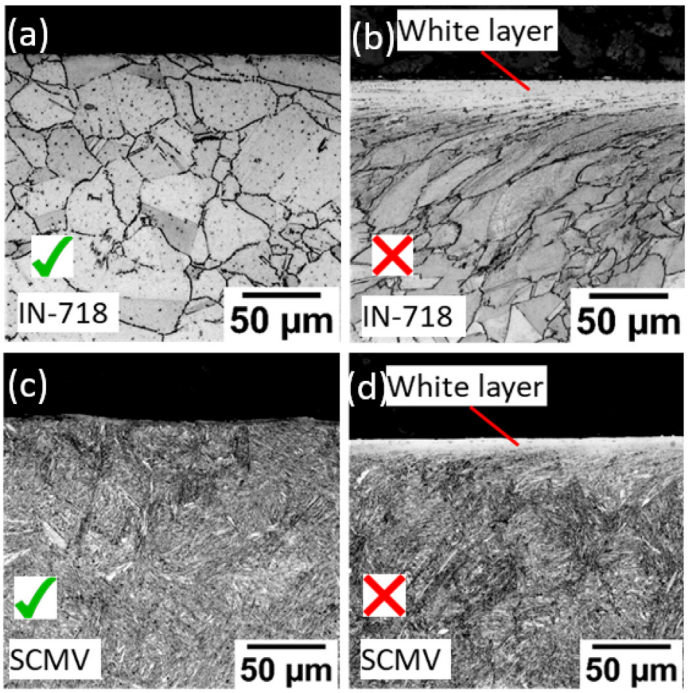

Fig. 10. Micrographs of (a) ad Inconel-718 surface without a white layer and (b) with a white layer and (c) a SCMV surface without a white layer and (d) with a white layer.

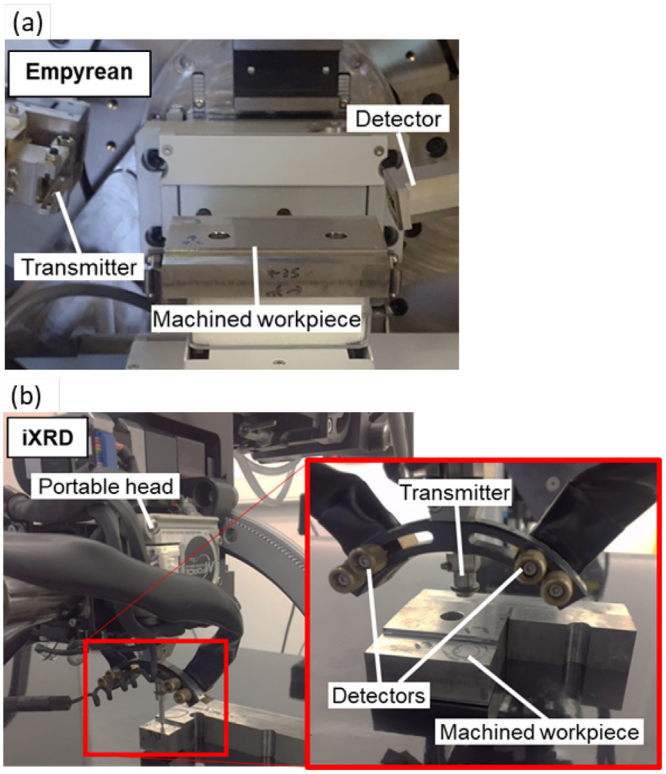

Fig. 11. Labelled photographs of (a) the Empyrean diffractometer and (b) the Proto iXRD portable diffractometer.

Table 4
Results from XRD-ΔPB measurements using equipment that facilitates truly non-destructive detection of Ti-6Al-4 V white layers.

Surface	Peak breadth Empyrean (°)	Peak breadth iXRD (°)
As-received	0.24	2.43
Machined no white layer	0.28	3.01
Machined white layer	0.41	3.55

unsurprising as small grain size and high lattice strain are intrinsic properties of these severely plastically deformed white layers and are therefore independent of the alloy under inspection. The sensitivity of the XRD-ΔPB method to nanoscale grains should also facilitate the detection of white layers formed through the phase transformation mechanism, due to their comparable ultrafine grain size [3].

A simple peak breadth threshold can be used to indicate the presence of a white layer depending on the alloy under inspection, the diffraction peak, the x-ray radiation and the diffractometer set-up. The increase in peak breadth for a surface containing a white layer is due to both crystallite size and inhomogeneous lattice strain broadening, as indicated from the results of the W-H analysis and the known ultrafine grain size within the white layers [4]. The inspection of electropolished surfaces with thin white layers highlights that peak breadth is related to white layer thickness when the x-ray penetration depth exceeds the layer thickness. However, it should be noted that the peak breadth values of the electropolished surfaces cannot be compared directly to as-machined surfaces, due to the redistribution of internal strain that occurs with layer removal. It is expected that as-machined surfaces containing a white layer would show a similar decay of peak breadth with decreasing white layer thickness, due to increased contribution from non-white layer material with a lower peak breadth, however, further work is required to be able to size white layers using peak breadth measurements. This is because, for the electropolished samples, different peak breadths can be associated with surfaces containing similar thicknesses of white layer.

The variation in peak breadth for crystallographic planes with similar diffraction angles, such as the $\alpha\{11\bar{2}0\}$ and $\alpha\{20\bar{2}0\}$ planes, as shown in Fig. 3, is a consequence of anisotropic peak broadening. The anisotropic broadening can be caused by strain anisotropy, which Shafi and Bose [29] have related to the elastic moduli of different crystallographic orientations, however, this is corrected for in the modified W-H method employed in this study. The residual anisotropy can be attributed to the orientation of the x-ray diffraction vector compared to the dislocation line vector in a crystal lattice, i.e. a dislocation orientation factor. This orientation difference can lead to anisotropic peak broadening when different types of dislocations are responsible for the lattice strain in grains of different orientations, as reported by Wilkens [34]. Due to the high levels of SPD in the white layer, the activation of many different slip systems, depending on grain orientation,

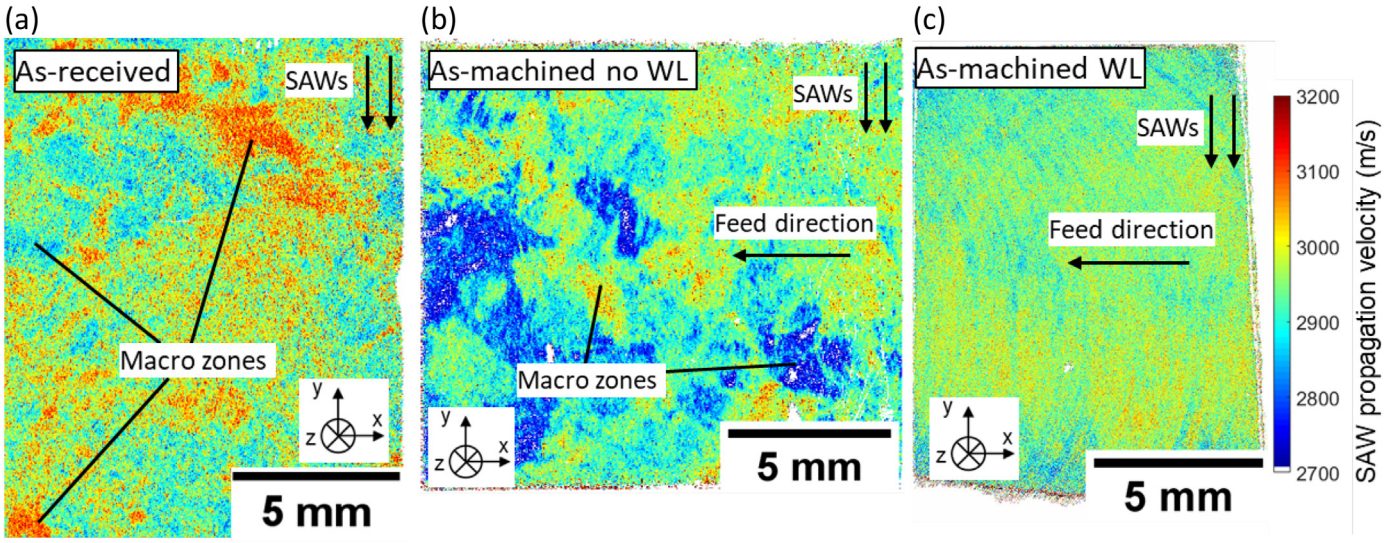

Fig. 12. SRAS velocity maps for (a) as-received cross-rolled Ti-6Al-4 V, (b) a machined surface with no white layer, (c) a machined surface that contains a white layer approximately 6 μm thick. Velocity scale consistent in each map.

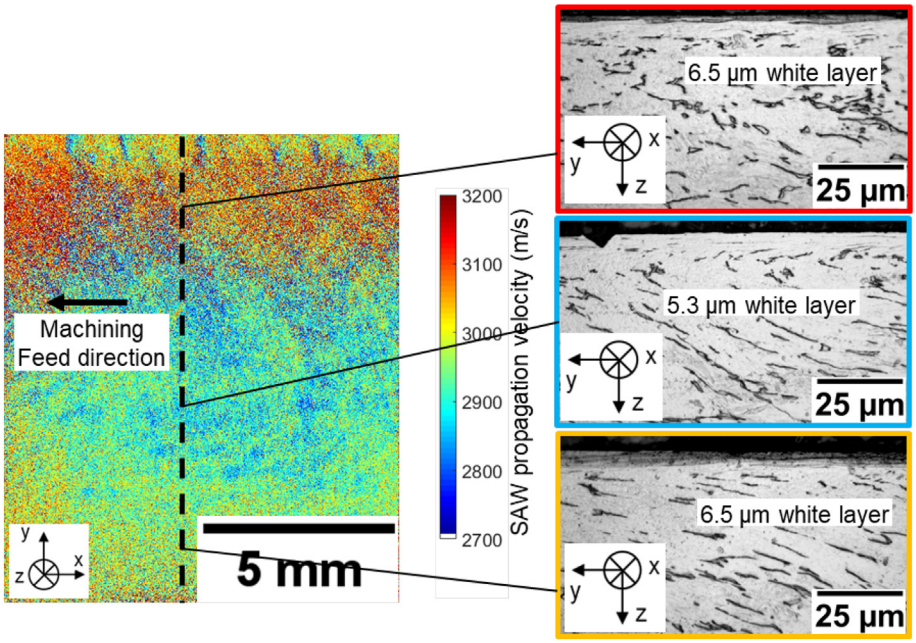

Fig. 13. A SRAS velocity map of a machined surface sample and the corresponding optical micrographs from a cross-sectional analysis of the surface using cutting direction samples.

is to be expected, resulting in considerable anisotropic strain broadening as can be seen in Fig. 9.

It can be seen from Fig. 3 that the α{0002} peak and the 2nd order α{0004} peak show no increase in FWHM for a surface with a white layer. This can be attributed to the basal texture of the white layers in addition to a change in the dislocation orientation factor for this plane, due to the deformation mechanisms that resulted in this texture. Crystallite size broadening effects may be reduced for the two planes

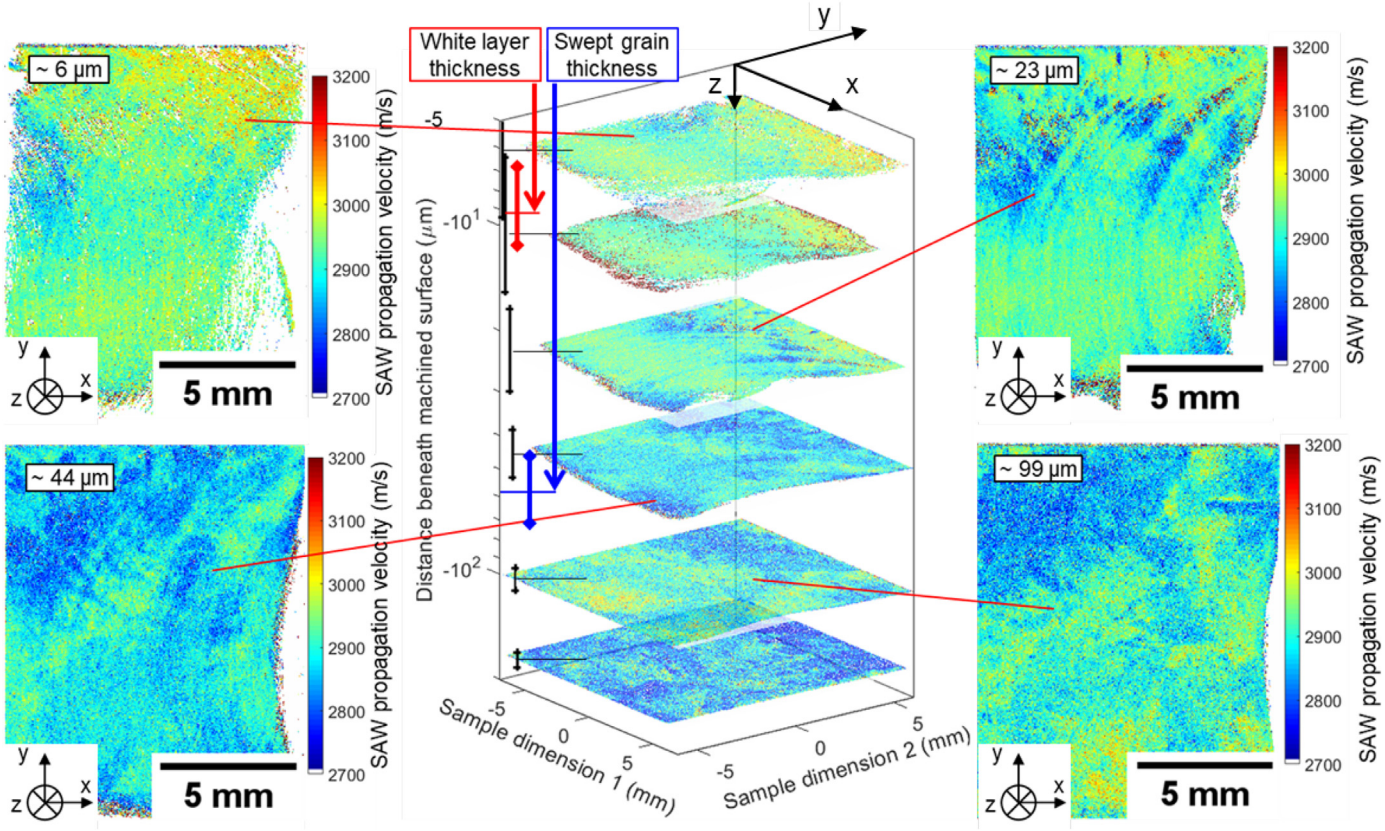

Fig. 14. SRAS velocity maps of machined surface samples at increasing depths facilitated by layer removal through electropolishing. The error bars represent the standard deviation of the depth measurement for each layer.

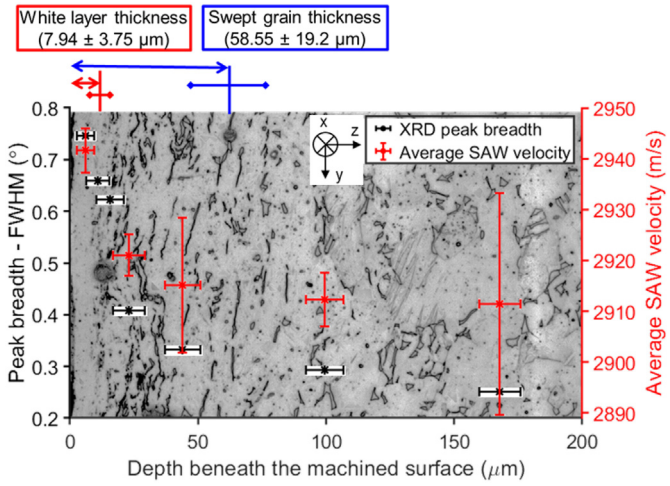

Fig. 15. The change in XRD peak breadth and average SRAS velocity with depth in a sample with a white layer. The plot is superimposed on a cross-sectional image, from a cutting direction sample, used to illustrate the white layer thickness.

identified, due to the presence of a large number of small grains with a basal orientation in a surface with a white layer, as the x-ray beam may interact with these small grains as if they were a single, large, basally-orientated grain.

In Ti-6Al-4 V, it is apparent that the strong basal texture of the white layers [4], results in a high-intensity α{0002} peak and the ratio of the intensity of this peak to that of a peak such as the $\alpha\left\{10\bar{1}1\right\}$ peak can be used as an indicator for the presence of a white layer. In all Ti-6Al-4 V samples inspected, an intensity ratio exceeding 1.9 was indicative of an anomalous surface with the method insensitive to as-received material with a basal orientation. The absence of a relationship between the IR and the white layer thickness in the Ti-6Al-4 V electropolished samples that possessed white layers thinner than the x-ray inspection depth is unsurprising, as it has previously been shown for machined titanium that the strength of the texture (the texture index of the pole figure orientation distribution function) is not proportional to the white layer thickness [4].

Although the XRD-ΔIR method is effective in Ti-6Al-4 V and IN-718 samples, it is not suitable for white layer detection in all aeroengine materials. This is because the texture in the white layer is not a fundamental physical property of the white layer itself, instead, it is a consequence of the deformation modes and the processing history for a particular material. As such the texture of the white layer is alloy-dependant, as evidence by the shear texture which has been reported for a nickel superalloy white layer [35] and the recrystallised texture that has been measured for a phase transformation white layer [36].

The results presented in Fig. 12 illustrate how SRAS data can be used to qualitatively differentiate between a surface with and without a white layer. The surfaces in Fig. 12(a) and (b) show clear signs of macrozones in which the underlying material microstructure causes changes in the SAW velocity. In Fig. 12(c) no distinguishable macrozones are present, instead, large arcs are observed in the SRAS velocity data which correspond to the path of the cutting tool over the workpiece surface as illustrated in Fig. 16. The difference in the shape of the arcs between the optical image and the velocity map confirms that this was not a surface topography artefact but instead a representation of the material properties of the near-surface region of the material being inspected. The difference in the shape between the physical feed marks and the velocity map arcs arises due to the different levels of mechanical polishing. The near-surface region is dominated by rubbing on the final tool pass, as highlighted in Fig. 17(a) and (b), and at greater depths the effect of deformation during chip formation is dominant and as such the shape of the arcs can change with depth. For the velocity maps presented in Fig. 14, the arcs visible at 23 μm and 44 μm depth were in the opposite direction to the surface topography arcs, with no clear arcs visible in either direction for the 6 μm map. The absence of clear arcs at 6 μm is thought to be due to averaging over a volume of material that contains deformation in one direction near the surface and in the opposite direction at greater depth, as can be seen by the representative micrograph in Fig. 17(b).

The subtle variation in the measured SAW velocities along the vertical axis of the velocity map in Fig. 12(c) was investigated further using cross-sectional micrographs along this axis. Fig. 13 illustrates how these changes in the group SAW velocity corresponded to the changes in the thickness of the white layer present on the surface. It is worth noting however that the SAW wavelength of 24 μm was much greater than the maximum white layer thickness of 6.5 μm measured in Fig. 13. This meant that with respect to Fig. 2, the SAW velocity measured was primarily influenced by the swept grain region below the white layer.

The SRAS results from progressive depths of the machined sample illustrated in Fig. 14 showed how SRAS provided a quantitative picture of the existence of the white layer and swept grain region. It was shown in Fig. 14 that with increasing material removal, the underlying

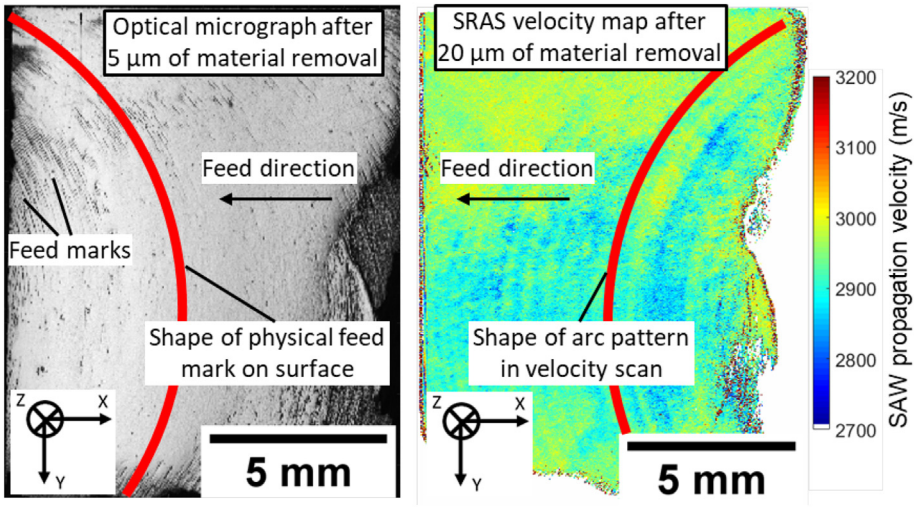

Fig. 16. An optical micrograph of the machined surface after 5 μm of material removal and a SRAS velocity map of the same surface after 20 μm of material removal. It can be seen that the shape of the feed marks in the optical micrograph is in the opposite direction to the arcs visible in the velocity map at greater depth.

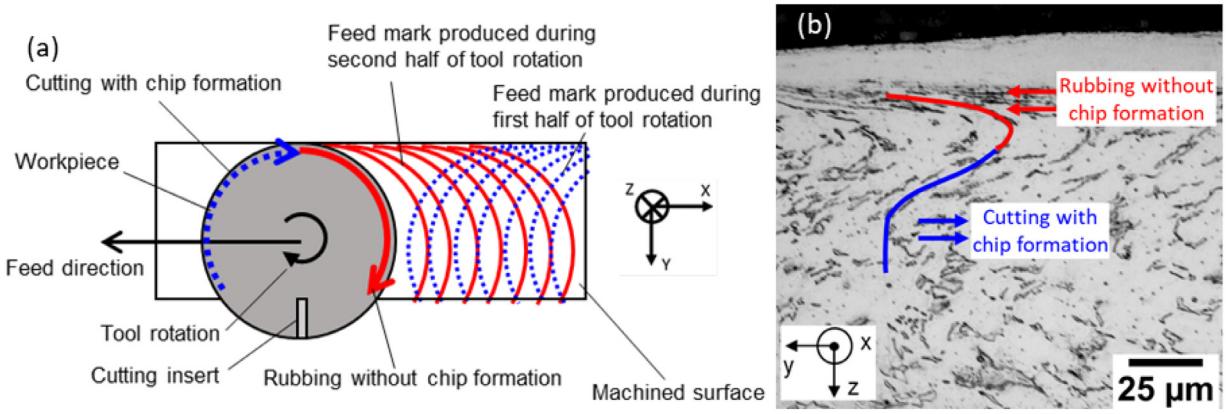

Fig. 17. A schematic (a) of the different regions of the cutting tool rotation and the corresponding arc shapes and (b) an illustrative cross-sectional optical micrograph highlighting the change in deformation direction with depth.

macrozones in the bulk microstructure became more prevalent in the SRAS data.

White layer detection through XRD-ΔPB measurements offers improvements over the current destructive process used in industry by avoiding the need to sacrifice parts for white-layer inspection. The non-destructive inspection can be carried out in a matter of minutes rather than the considerable time required for sectioning, micro-preparation, etching, microscopy and analysis during destructive inspection methods. Scanning electron microscopy, rather than optical microscopy, would typically be required to verify the presence of a sub-5 μm white layer, due to uncertainties introduced by edge-rounding during sample preparation and un-even etching if a sample is contaminated. As such, there is a minimal detectable thickness in the region of 5 μm for white layers inspected with optical microscopy. Results presented in this study have shown that XRD methods can offer improved resolution capability compared to the existing optical inspection method in a fraction of the time, thereby offering a step-change in the inspection of machining-induced white layers. To expand the capabilities of this technique, future work should investigate the inspection of as-machined white layers thinner than 5 μm and investigate the potential for other surface integrity features via changes in peak broadening due to the level of plastic strain in a surface.

The SRAS results presented show the initial steps taken towards quantitatively measuring the thickness of the white layer and swept grain region. Compared to the current destructive process, a laser ultrasonic technique such as SRAS could be used to carry out such an inspection on a machined (rough) surface non-destructively, as shown in the literature [25]. The capability of SRAS to carry out on the fly measurements gives it a distinct advantage over point-based methods but is currently limited by laser repetition rate and mechanical stage speed. The combination of this rough surface capability and on the fly measurement makes SRAS an ideal candidate for the in-situ inspection of machining processes enabling closed-loop feedback and extremely efficient tooling decisions. Future work in this technique should aim to attempt to utilise higher frequencies to reduce the inspection depth thereby increasing the signal to noise ratio for a thin surface white layer.

5. Conclusions

This research was undertaken to investigate the potential to non-destructively inspect for machining-induced white layers in aeroengine alloys. This study introduces a novel x-ray diffraction-based approach for truly non-destructive surface integrity inspection that has been validated for the three major aeroengine material groups. The technique offers a resolution, in terms of detectable white layer thickness, that competes with the current destructive process but with a significant reduction in inspection time, from days or hours down to minutes. Measurements using the emerging SRAS technology have shown that surface acoustic wave methods may also be suitable for white layer detection and may additionally offer identification of swept grain material, another important feature assessed during surface integrity assessment. The key findings of the work can be summarised as follows:

- XRD-ΔPB measurements can be used to reliably and rapidly detect machining-induced white layers in all key aeroengine material groups due to the ultrafine grain size and high lattice strain in the white layer. These intrinsic properties of white layers, which are present in ferromagnetic and non-ferromagnetic materials, cause x-ray diffraction peak broadening. It was shown that when peak broadening is larger than would be expected in a normal machined surface, the presence of a white layer can be inferred.
- XRD-ΔIR measurements can also be used to detect white layers in Ti-6Al-4 V and Inconel-718. In this method, the intensity ratio between particular peaks can be used to infer the presence of a white layer if it exceeds the values expected from a surface without a white layer. A high intensity ratio is due to the strong crystallographic textures of the white layers in these materials, but the technique is not transferable to all aeroengine materials as the crystallographic texture is not consistent across material groups.
- The XRD-ΔPB method offers the potential for comparable or greater resolution than the current destructive optical microscopy method whilst significantly reducing inspection time and removing the need to sacrifice the component. This is partly due to the inherently small penetration depth of x-rays into the machined surface which is of the order of typical white layer thicknesses.
- Compared to other NDT techniques which have been proposed for white layer detection, the XRD-ΔPB method is applicable across alloy groups and is sensitive to an intrinsic property of the white layer, rather than residual stress, for example, which can vary significantly between different white layers.
- The SRAS method is sensitive to both white layer and swept grain material within the inspection volume and can be used to qualitatively indicate the presence of an anomalous surface in Ti-6Al-4 V. SRAS is sensitive the crystallographic texture and as such, anomalous surfaces can be identified from the destruction of the macroscopic texture visible in a velocity map which occurs during a machining operation that forms a white layer.

Data availability

The raw/processed data required to reproduce these findings cannot be shared at this time as the data also forms part of an ongoing study.

Declaration of Competing Interest

The authors declare that they have no known competing financial interests or personal relationships that could have appeared to influence the work reported in this paper.

Acknowledgements

This research was supported by Rolls-Royce and Seco Tools in addition to the EPSRC [grant numbers EP/L016257/1, and EP/S013385/1].

References

[1] E.O. Ezugwu, J. Bonney, Y. Yamane, An overview of the machinability of aeroengine alloys, J. Mater. Process. Technol. 134 (2) (2003) 233–253, Art no. Pii s0924–0136 (02)01042–7. Mar https://doi.org/10.1016/s0924-0136(02)01042-7.
[2] C.H. Che-Haron, A. Jawaid, The effect of machining on surface integrity of titanium alloy Ti–6% Al–4% V, J. Mater. Process. Technol. 166 (2) (2005) 188–192, https://doi.org/10.1016/j.jmatprotec.2004.08.012.
[3] B.J. Griffiths, Mechanisms of white layer generation with reference to machining and deformation processes, J. Tribol. 109 (3) (1987) 525–530, https://doi.org/10.1115/1.3261495.
[4] M. Brown, et al., Quantitative characterization of machining-induced white layers in Ti–6Al–4V, Mater. Sci. Eng. A 764 (2019) 138220, 2019/09/09/ https://doi.org/10.1016/j.msea.2019.138220.
[5] J. Kwong, D.A. Axinte, P.J. Withers, The sensitivity of Ni-based superalloy to hole making operations: influence of process parameters on subsurface damage and residual stress, J. Mater. Process. Technol. 209 (8) (2009) 3968–3977, https://doi.org/10.1016/j.jmatprotec.
[6] C. Herbert, D.A. Axinte, M. Hardy, P. Withers, Influence of surface anomalies following hole making operations on the fatigue performance for a Nickel-based superalloy, J. Manuf. Sci. Eng. 136 (5) (2014) https://doi.org/10.1115/1.4027619 051016 1–9.
[7] G. Poulachon, A. Albert, M. Schluraff, I.S. Jawahir, An experimental investigation of work material microstructure effects on white layer formation in PCBN hard turning, Int. J. Mach. Tools Manuf. 45 (2) (2005) 211–218, https://doi.org/10.1016/j.ijmachtools.2004.07.009.
[8] M.C. Hardy, et al., Characterising the integrity of machined surfaces in a powder nickel alloy used in aircraft engines, Procedia CIRP 13 (Supplement C) (2014) 411–416, https://doi.org/10.1016/j.procir.2014.04.070.
[9] M. Brown, et al., Destructive and non-destructive testing methods for characterization and detection of machining-induced white layer: a review paper, CIRP J. Manuf. Sci. Technol. 23 (2018) 39–53.
[10] A. Stupakov, M. Neslušan, O. Perevertov, Detection of a milling-induced surface damage by the magnetic Barkhausen noise, J. Magn. Magn. Mater. 410 (2016) 198–209, 2016/07/15/ https://doi.org/10.1016/j.jmmm.2016.03.036.
[11] M. Brown, et al., Non-destructive detection of machining-induced white layers in ferromagnetic alloys, Procedia CIRP 87 (2020) 420–425.
[12] S.B. Hosseini, U. Klement, Y. Yao, K. Ryttberg, Formation mechanisms of white layers induced by hard turning of AISI 52100 steel, Acta Mater. 89 (2015) 258–267, https://doi.org/10.1016/j.actamat.2015.01.075.
[13] Y.B. Guo, S.C. Ammula, Real-time acoustic emission monitoring for surface damage in hard machining, Int. J. Mach. Tools Manuf. 45 (14) (2005) 1622–1627, https://doi.org/10.1016/j.ijmachtools.2005.02.007.
[14] L. Daghini, et al., Non Destructive Testing Methods: Development of Innovative Solutions for in-Line Applications, FPI suatainable production 2014.
[15] T. Patton, et al., Nondestructuve Evaluation of Manufacturing Induced Anomalies - DOT/FAA/AR-10/32, U.S. Department of Transportation Federal Aviation Administration, 2011.
[16] B.D. Cullity, *Elements of X-Ray Diffraction, Addison* (Wesley Mass), 1978.
[17] A. Zhilyaev, et al., Microstructural characterization of ultrafine-grained nickel, Phys. Status Solidi A 198 (2) (2003) 263–271.
[18] T. Ungár, G. Tichy, J. Gubicza, R. Hellmig, Correlation between subgrains and coherently scattering domains, Powder Diffract. 20 (4) (2005) 366–375.
[19] G. Baumann, H. Fecht, S. Liebelt, Formation of white-etching layers on rail treads, Wear 191 (1–2) (1996) 133–140.
[20] F. Larson, A. Zarkades, Properties of textured titanium alloys, Technical Report - Battelle Columbus Labs Ohio Metals and ceramics information Centre 1974, p. 15.
[21] G. Farnell, Properties of elastic surface waves, Phys. Acoust. 6 (1970) 109–166.
[22] R.J. Smith, M. Hirsch, R. Patel, W. Li, A.T. Clare, S.D. Sharples, Spatially resolved acoustic spectroscopy for selective laser melting, J. Mater. Process. Technol. 236 (2016) 93–102, https://doi.org/10.1016/j.jmatprotec.2016.05.005.
[23] L.-S. Wang, J.S. Steckenrider, J.D. Achenbach, A fiber-based laser ultrasonic system for remote inspection of limited access components, in: D.O. Thompson, D.E. Chimenti (Eds.), Review of Progress in Quantitative Nondestructive Evaluation: Volume 16A, Springer US, Boston, MA 1997, pp. 507–514.
[24] M. Dubois, M. Militzer, A. Moreau, J.F. Bussière, A new technique for the quantitative real-time monitoring of austenite grain growth in steel, Scr. Mater. 42 (9) (2000).
[25] R. Patel, et al., Imaging material texture of as-deposited selective laser melted parts using spatially resolved acoustic spectroscopy, Appl. Sci. 8 (10) (2018) 1991.
[26] R.J. Smith, W. Li, J. Coulson, M. Clark, M.G. Somekh, S.D. Sharples, Spatially resolved acoustic spectroscopy for rapid imaging of material microstructure and grain orientation, Meas. Sci. Technol. 25 (5) (2014), [Online]. Available: http://stacks.iop.org/0957-0233/25/i=5/a=055902.
[27] S.D. Gates-Rector, T.N. Blanton, The powder diffraction file: a quality materials characterization database, Powder Diffract. 34 (2019) 352–360.
[28] P. Scardi, M. Leoni, R. Delhez, Line broadening analysis using integral breadth methods: a critical review, J. Appl. Crystallogr. 37 (3) (2004) 381–390.
[29] P. Muhammed Shafi, A. Chandra Bose, Impact of crystalline defects and size on X-ray line broadening: A phenomenological approach for tetragonal SnO2 nanocrystals, AIP Adv. 5 (5) (2015) 057137.
[30] J.H. Hubbell, Photon mass attenuation and energy-absorption coefficients, The International Journal of Applied Radiation and Isotopes 33 (11) (1982) 1269–1290.
[31] A.F. Mark, W. Li, S. Sharples, P.J. Withers, Comparison of grain to grain orientation and stiffness mapping by spatially resolved acoustic spectroscopy and EBSD, J. Microsc. 267 (1) (2017) 89–97, https://doi.org/10.1111/jmi.12550.
[32] C.B. Scruby, L.E. Drain, Laser Ultrasonics Techniques and Applications, CRC press, 1990.
[33] R. Patel, W. Li, R.J. Smith, S.D. Sharples, M. Clark, Orientation imaging of macro-sized polysilicon grains on wafers using spatially resolved acoustic spectroscopy, Scr. Mater. 140 (2017) 67–70.
[34] M. Wilkens, X-ray line broadening and mean square strains of straight dislocations in elastically anisotropic crystals of cubic symmetry, Phys. Status Solidi A 104 (1) (1987) K1–K6.
[35] R. M'Saoubi, et al., Surface integrity analysis of machined Inconel 718 over multiple length scales, CIRP Ann. 61 (1) (2012) 99–102.
[36] V. Bedekar, R. Shivpuri, A. Avishai, R.S. Hyde, Transmission Kikuchi Diffraction study of texture and orientation development in nanostructured hard turning layers, CIRP Ann. 64 (1) (2015) 73–76 , 2015/01/01/ https://doi.org/10.1016/j.cirp.2015.04.073.